Hydrogen-catalyzed acid-transformation for the hydration of alkenes and epoxy alkanes over Co-N frustrated Lewis pair surface

Qiang Deng[1]†, Xiang Li[1]†, Ruijie Gao[2,3]†, Jun Wang[1], Zheling Zeng[1], Ji-Jun Zou[2]*, Shuguang Deng[4]*, Shik Chi Edman Tsang[5]*

[1]School of Resource, Environmental and Chemical Engineering, Nanchang University, Nanchang 330031, PR China

[2]School of Chemical Engineering and Technology, Tianjin University, Tianjin 300072, PR China

[3]Engineering Research Center of Nano-Geomaterials of Ministry of Education, China University of Geosciences, Wuhan 430074, PR China

[4]School for Engineering of Matter, Transport and Energy, Arizona State University, Tempe, AZ 85287, USA

[5]Wolfson Catalysis Centre, Department of Chemistry, University of Oxford, Oxford OX1 3QR, UK

*Corresponding Authors. E-mail: edman.tsang@chem.ox.ac.uk; Shuguang.Deng@asu.edu; jj_zou@tju.edu.cn.

† The authors contributed equally to this work.

KEYWORDS: Co-N pairs, H_2 catalysis, acid transformation, hydration, hydrogenation

ABSTRACT: Hydrogen (H_2) is widely used as a reductant for many hydrogenation reactions; however, it has not been recognized as a catalyst for acid transformation of active sites on solid surface. Here, we report the H_2-promoted hydration of alkenes (such as styrenes and cyclic alkenes) and epoxy alkanes over single atom Co dispersed nitrogen-doped carbon (Co-NC) via a transformation mechanism of acid-base sites. Specifically, the specific catalytic activity and selectivity of Co-NC are more superior to those of classical solid acids (acidic zeolites and resins) per μmol of acid, whereas the hydration catalysis does not take place in a nitrogen atmosphere. Detailed investigations indicate that H_2 can be heterolyzed on the Co-N to form $H^{\delta-}$-Co-N-$H^{\delta+}$ and then converted into $OH^{\delta-}$-Co-N-$H^{\delta+}$ accompanied by H_2 generation via a H_2O-mediated path, which significantly reduces the activation energy for hydration reactions. This work not only provides a novel catalytic method for hydration reactions but also removes the conceptual barriers between hydrogenation and acid catalysis.

Introduction

Molecular hydrogen (H_2) is the most common reductant in various catalytic hydrogenation reactions. The dissociative adsorption of H_2 is often homolytic cleavaged to H atoms over transition metal catalysts (Scheme 1A) [1-3], but a heterolysis activation mechanism of H_2 to $H^{\delta+}$ and $H^{\delta-}$ has been accepted for "frustrated Lewis acid-base pairs" (FLP) with a polarized electronic structure such as B-P, B-N, Fe-P, Co-N (Scheme 1B) [4-9]. Specifically, Co-N is highly efficient for the H_2 activation and hydrogenation of asymmetric unsaturated bonds such as carbonyl, nitro, and cyano groups [10-13]. At the same time, acid catalysis is also widely used in numerous reactions, for which the acid type (Lewis or Brønsted) and acid strength usually have a considerable influence on the catalytic activity [14-16].

In most cases, acid and hydrogenation catalysis seems to be uncorrelated with each other, and the role of H_2 has rarely been considered in acid catalysis. For example, in many tandem reactions using metal/acidic support bifunctional catalysts, such as hydrodeoxygenation, hydrodesulfurization, and hydrogenative etherification, it is generally considered that the roles of transition metals and acidic supports are responsible for hydrogenation and acid catalysis, respectively [17-19]. As a special case, over noble metal/reductive metal oxides (such as Pt/WO_3-ZrO_2 and Pt/MoO_3-ZrO_2), H_2 can be hemolytic to H atoms over noble metals and spill to the reductive support [20-25]. Hydrogen spillover can cause the acid transformation of Lewis to Brønsted acidity via the generation of proton hydrogen (H^+) and the reduction of the valence of metal ions on the support (Scheme 1C). Theoretically, the so-called "H_2-induced" acid transformation can modulate the catalytic activity of many acid-catalyzed reactions. However, due to the high reaction temperature and the use of noble metals, their acid-catalyzed ability has rarely been reported and has only achieved limited success in alkane isomerization [20-24] and ethylbenzene disproportionation [25]. In fact, H_2 also plays a role of a reductant in the H_2-induced acid transformation process.

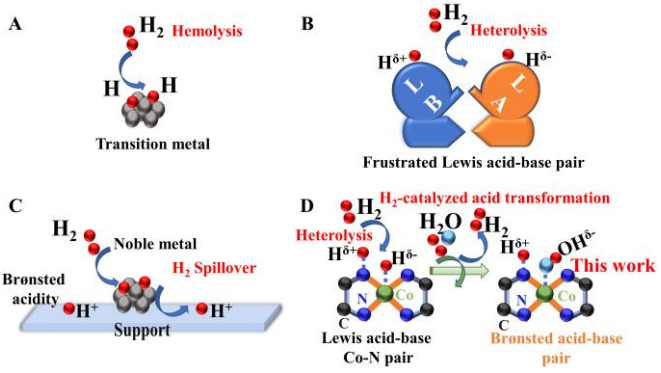

Scheme 1. Hydrogen reaction mechanism.

Recently, single-atom catalysts have attracted wide attention in heterogeneous catalysis due to unique properties compared with conventional nanoparticle catalysts [26-28]. Herein, single atom Co dispersed nitrogen-doped carbon (Co-NC) on surface was prepared via pyrolysis of double metal cyanide and followed by acid treatment. We found that H_2 can be heterolytically dissociated over the frustrated Lewis acid-base Co-N pair to $H^{\delta-}$-Co-N-$H^{\delta+}$ and then transformed into a Brønsted acid-base $OH^{\delta-}$-Co-N-$H^{\delta+}$ pair accompanied by H_2

regeneration via a H_2O-mediated path (Scheme 1D). Interestingly, H_2 plays the role as a catalyst for the conversion of acid-base properties of solid catalyst, rather than the common role of a reductant. The H_2 catalytically generated $OH^{\delta-}$-Co-N-$H^{\delta+}$ shows a better catalytic performance than traditional acidic zeolites (HZSM-5, Hβ) and resins (Amberlyst-15) in the hydration of alkenes (including styrenes and cyclic alkenes) to alcohols and epoxy alkanes to diols.

Materials and Methods

Synthesis of Co-NC

The details of the chemical reagents are shown in the Supporting Information. The double metal cyanide $Zn_3[Co(CN)_6]_2$ was synthesized via a simple precipitation method [29]. Briefly, 0.012 mol of potassium hexacyanocobaltate ($K_3Co(CN)_6$) was dissolved in 70 mL of water. Next, 0.09 mol of zinc chloride ($ZnCl_2$) was dissolved in 20 mL of water, which was slowly added to the former solution in 1 h at 50 °C under vigorous stirring. Then, 15.0 g of poly(ethylene glycol)-block-poly(propylene glycol)-block-poly-(ethylene glycol) (P_{123}, average molecular weight=5800) and 40 mL of tert-butanol were added in 10 min and stirred continuously for 1 h. Subsequently, the resultant white solid was collected and washed with water and ethanol to remove the unreacted ions, and then dried at 120 °C for 8 h. Similarly, double metal cyanide $Co_3[Co(CN)_6]_2$ was prepared by an identical method except for changing $ZnCl_2$ to cobaltous nitrate ($Co(NO_3)_2$) [30].

Then, $Zn_3[Co(CN)_6]_2$ was heated to 900 °C for 2 h with a heating rate of 3 °C/min under a N_2 atmosphere to obtain Co nanoparticle-supported nitrogen-doped carbon layer Co@Co-NC. Then, 0.1 g of Co@Co-NC was added to 30 mL of H_2SO_4 aqueous solution (2.0 M) and heated at 50 °C for 12 h under vigorous stirring. The Co nanoparticles were removed, and a single atom Co dispersed nitrogen-doped carbon Co-NC was synthesized. Finally, the resultant solid was collected by washing with water until the pH of the filtrate reached 7.0 and then dried at 120 °C for 8 h. Details of the characterization of the catalyst are provided in the Supporting Information.

Catalytic reactions

The hydration of alkenes and epoxy alkanes was performed in a 25.0 mL batch autoclave (Anhui Kemi Machinery Technology Co., LTD). Typically, the reaction was carried out with 10 mmol of substrate, 10 mL of solvent, and solid acids with an acid amount of 8.0 μmol at 150 °C and 4.0 MPa H_2 pressure. Then, the reaction mixture was sampled periodically, and 20 μL of N,N-dimethylformamide was used as an internal standard substance. The products were determined by an Agilent 6890 N GC/5973 MS detector and quantified by a gas chromatograph (Trace 1300) installed with an FID detector and a TG-WAXMS capillary column (30 m × 0.32 mm × 0.25 μm). The ^1H NMR spectra of the reaction products were collected on a Varian Inova 500 MHz NMR using D_6-benzene as a solvent.

Density functional theory (DFT) calculations

All density functional theory calculations were carried out with the Vienna Ab initio Simulation Package (VASP) [31,32]. The exchange-correlation functional employed was the Perdew-Burke-Ernzerhof (PBE) functional of the generalized gradient approximation. The kinetic energy cutoff of 500 eV was employed. The Brillouin zone was sampled using a Monkhorst-pack 4 × 4 × 1 k-point grid for active site CoN_4 and 4 × 3 × 1 for CoN_{2+2}. The transition state of chemical reactions was located using the climbing image nudged elastic band (CI-NEB) method with a convergence of 0.05 eV/A for the force components both along and perpendicular to the tangent of the reaction path. The vacuum region was 20 Å. All of the structures were optimized until the force on each atom was less than 0.02 eV/Å. The adsorption energies, E_{ads}, are calculated by using the following equation:

$$E_{ads} = E_{adsorbate+surface} - (E_{adsorbate} + E_{surface})$$

where E_{ads} is the adsorption energy, $E_{adsorbate+surface}$ is the total energy of the surface covered with adsorbates, $E_{surface}$ is the energy of the clean surface, and $E_{adsorbate}$ is the energy of the adsorbate. The electrolyte was incorporated implicitly with the Poisson-Boltzmann model implemented in VASPsol [33]. The dielectric constant was set to 78.4 for H_2O [34].

Results and Discussion

Characterizations of Co-NC

The synthetic process of Co-NC is shown in Figure 1A. Inductively coupled plasma optical emission spectrometry (ICP-OES) indicates that the Zn element of $Zn_3[Co(CN)_6]_2$ is completely evaporated during the carbonizing process, and the C, N, and Co elements serve as carbon, nitrogen and Co sources for the formation of Co@Co-NC (Table S1). X-ray diffraction (XRD) patterns and transmission electron microscopy (TEM) images show the physicochemical structure changes of $Zn_3[Co(CN)_6]_2$ after high-temperature carbonization at 900 °C in a N_2 atmosphere to prepare Co@Co-NC (Figure S1) [29]. The broad and weak peak of C (002) located at 25.8° can be assigned to the existence of Co-dispersed nitrogen-doped graphene layers, and the diffraction peaks located at 2θ= 44.3°, 51.5°, and 76.1° are assigned to the (111), (200), and (220) planes of the standard card of face-centered cubic Co (JCPDS No. 15-0806) [35]. After the acid treatment, XRD and TEM results show that the characteristic signals of Co nanoparticles are removed and Co-dispersed nitrogen-doped carbon remains. Energy-dispersive X-ray spectroscopy (EDS) mappings revealed the homogeneous distributions of Co, N and C elements in the Co-NC catalyst (Figure S1). Based on the N_2 adsorption-desorption isotherm, Co-NC possesses a large BET surface area of 154.6 m^2/g and pore volume of 0.273 cm^3/g (Figure S2, Table S1). ICP-OES and Raman spectra indicate a 1.0 wt% Co content in graphitized carbon (Table S1, Figure S3). High-angle annular dark-field scanning transmission electron microscopy (HAADF-STEM) images suggest isolated and well-dispersed Co atoms (Figure 1B, C). To investigate the coordination environment of Co species at the atomic level, the Co K-edge X-ray absorption near-edge structure (XANES) of Co-NC was compared with the reference samples (Figure 1D). The coordination environment was demonstrated by the extended X-ray absorption fine structure (EXAFS) spectrum, and the Fourier transform (FT) k3-weighted χ(k) EXAFS (FT-EXAFS) spectrum of Co-NC showed a main peak at 1.6 Å that perfectly matched the Co-N_4 structure (Figure 1E) [36]. Notably, no Co-Co coordination peak was observed at 2.18 Å, which unambiguously implied the complete absence of Co nanoparticles. The chemical compositions of the obtained samples were investigated by X-ray photoelectron spectroscopy (XPS). The high-resolution N 1s spectra of Co-NC could be deconvoluted into pyridinic N (398.5 eV), pyrrolic N (399.8 eV), and graphitic N (401.2 eV) [37] (Figure 1F). Meanwhile, the Co 2p peaks focused at 796.0 and 780.1 eV, in addition to correlated satellite peaks (802.2 and 783.9 eV), can be well ascribed to the $2p_{1/2}$ and $2p_{3/2}$ of Co-N bonding, respectively (Figure 1G). The Co $2p_{3/2}$ peak at 780.1 eV indicates that Co has an oxidation state between 0 and +2, which is tetracoordinated with pyridinic N atoms [38].

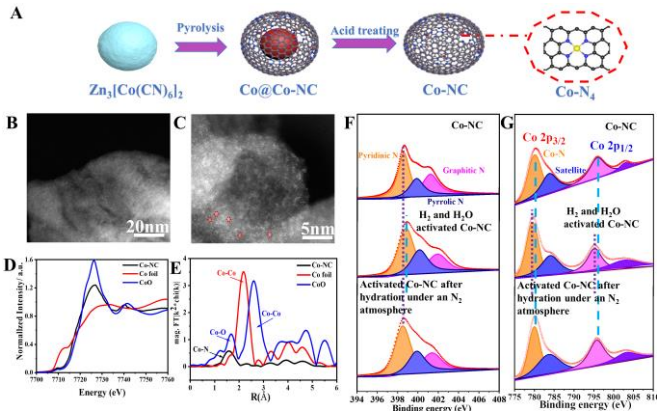

Figure 1. (A) Synthesis procedures of Co-NC; (B, C) Aberration-corrected HAADF-STEM images with accompanying EELS point spectra of Co-NC; (D) Normalized Co K-edge XANES spectra of Co-NC and referenced CoO and Co foil; (E) FT-EXAFS spectra of Co-NC, CoO, and Co foil; (F) N 1s and (G) Co 2p XPS spectra of the parent, H_2-H_2O activated Co-NC and activated Co-NC after hydration reaction under an N_2 atmosphere.

Alkene hydration to alcohols

Figure 2A and Table 1 entry 1 exhibit the results of the hydration of 3-chlorostyrene to 1-(3-chlorophenyl)ethanol using Co-NC as the catalyst. Under a H_2 atmosphere, Co-NC achieves 89.3% conversion of 3-chlorostyrene and 99.5% selectivity to 1-(3-chlorophenyl)ethanol in H_2O solvent. Control experiments show that no 3-chlorostyrene is converted over Co-NC under a N_2 atmosphere or under a H_2 atmosphere in the absence of Co-NC. Furthermore, only the hydrogenated product, i.e., 3-chlorophenylethane is obtained when *n*-hexane were used as a solvent (Table 1 entry 2, 3). These results indicate that H_2 is indispensable for Co-NC catalytic hydration. Moreover, the hydrated product follows Markovnikov's rule (that is, proton and hydroxyl bonds to the primary and secondary carbon of the C=C bond, respectively), suggesting that the reaction follows the acid-catalyzed mechanism [39,40].

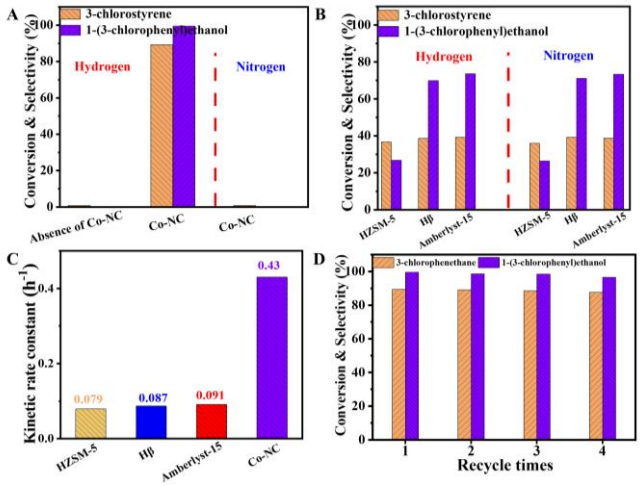

Figure 2. (A) The catalytic performance of Co-NC for 3-chlorostyrene hydration under different atmosphere; (B) The catalytic performance of conventional solid acid catalysts; (C) Kinetic rate constants of various catalysts under H_2 atomosphere; (D) Recycling performance of Co-NC. Reaction conditions: 3-chlorostyrene (10 mmol), catalyst (Co-NC 50 mg, ZSM-5 19.2 mg, Hβ 23.6 mg, Amberlyst-15 2 mg), water (10 mL), 150 °C, 4.0 MPa atmosphere, reaction time 6 h. Quantified by GC.

Some traditional solid acid catalysts (such as sulfonated resin amberlyst-15, acidic zeolites HZSM-5 and Hβ) were investigated. The acid properties of zeolites and Co-NC were determined by the temperature-programmed desorption of ammonia (NH_3-TPD), and the acid concentrations of HZSM-5, Hβ and Co-NC were 0.421, 0.341 and 0.161 mmol/g, respectively (Figure S4, Table S2). Meanwhile, the acid concentration of amberlyst-15 is 4.139 mmol/g, as detected by the acid-base titration [41]. As a comparison, the same acid amount of 8.0 μmol was used in the reaction. Compared with the Co-NC, HZSM-5, Hβ, and amberlyst-15 showed a relatively lower conversions of 36.7%, 38.6%, and 39.3%, respectively (Figure 2B). Meanwhile, a large amount of carbon loss of approximately 30-40% is generated via the polymerization side reaction, which decreases the selectivity for the target products [42]. The conversion over traditional solid acids is the same under a H_2 or N_2 atmosphere. Based on the time-dependent product distributions (Figure S5), the hydration reaction follows pseudo-first-order kinetics, and the specific kinetic rate constant of Co-NC is 5~6 times higher than those of traditional solid acids per μmol of acid (Figure 2C). Furthermore, Co-NC shows a stable performance in recycling runs, without distinct activity degradation (Figure 2D).

Table 1. Hydration of alkenes to alcohols.

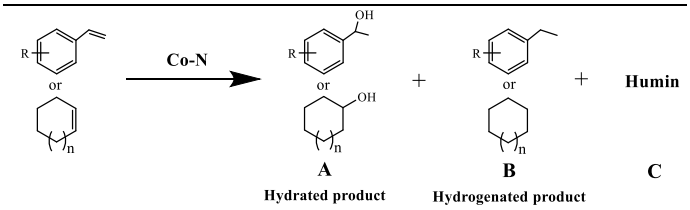

Entry	Alkenes	Conversion (%)	Selectivity (%)		
			A	B	C
1		89.3	99.5	-	0.5
2	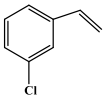	68.3		99.9	
3	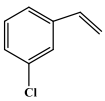	63.8		99.9	
4	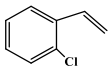	90.2	89.3	-	10.7
5		10.3	99.5	-	0.5
6		44.5	-	99.9	-
7		8.7	98.6	-	1.4
8		5.5	98.9		1.1
9	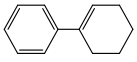	21.3	99.9	-	0.1
10	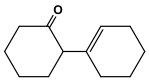	51.3	96.3	-	3.7
11		8.9	98.0	-	2.0
12		13.6	99.9	-	0.1

13		23.1	98.6	-	1.4
14		2.1	99.0	-	1.0

Reaction conditions: alkenes (10 mmol), Co-NC (50 mg), H_2O (10 mL), 150 °C, 4.0 MPa H_2, reaction time 6 h. [2,5]*n*-hexane instead of H_2O.[3]tetrahydrofuran. Quantified by GC.

The hydration of 11 other alkenes (including 2-chlorostyrene, cyclohexene, 1-methyl cyclohexene, 3-carbonyl cyclohexene, 1-phenyl cyclohexene, 1-(2-cyclohexanone)-cyclohexene, cyclopentene, cyclooctene, cyclododecene, and 1-hexene) is further explored, and the reaction is highly selective with the corresponding secondary alcohols or cyclic alcohols as major products (Table 1). It should be mentioned that sensitive functional groups such as aldehyde and ketone groups are well preserved without being reduced under the reaction conditions. Co-NC still shows a 90.2% conversion of 2-chlorostyrene, and 89.3% of target alcohols (Table 1 entry 4). However, for cyclic alkenes and linear alkenes, hydration is reversible, and equilibrium strongly affects the final conversion [42-47]. Typically, for the hydration of cyclohexene to cyclohexanol, the conversion is only 10.3% after 6 h (Figure 3A, Table 1 entry 5). Under the same conditions, almost the same amount of cyclohexene (10.2%) can be obtained using cyclohexanol as the reactant (Figure S6). Similarly, no reaction occurs under the N_2 atmosphere and H_2O solvent, and only hydrogenated product is generated under H_2 and *n*-hexane or sulfolane solvent (Table 1 entry 2, 3). In previous work, Zhang et al also found a pseudo first-order kinetic reaction based on aqueous phase concentrations of cyclohexene and cyclohexanol in an aqueous solution [43]. Also, the reaction was conducted by using sulfolane as a cosolvent to verfiy whether the increase in the solubility of cyclohexene in the aqueous phase can affect the kinetics: the cyclohexene hydration also follows a first-order kinetic with similar rate constant obtained, indicating that the solubility of the reactant in this reaction system may not be the limiting factor [48]. Meanwhile, a 12.5% selectivity of cyclohexane can be generated by the hydrogenation route. The catalytic activity of Co-NC is still higher than that of traditional solid acids (Figure 3A, Figure S6). Other alkenes also show reversible pseudo-first-order kinetics with equilibrium conversion of 2-60% (Table 1 entries 7-14) [39, 42-47, 49, 50].

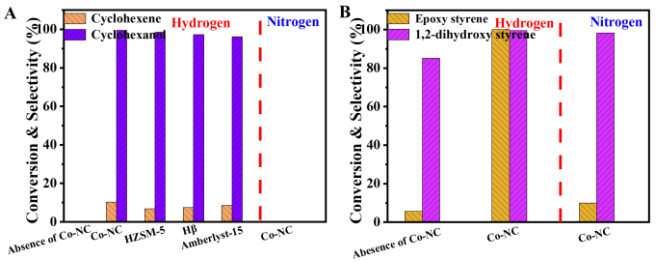

Figure 3. (A) The catalytic performance of cyclohexene hydration over different catalysts and atmosphere; (B) The catalytic performance of epoxy styrene hydration over Co-NC under different atmosphere. Reaction conditions: cyclohexene (A) or Epoxy styrene (B) (10 mmol), catalyst (Co-NC 50 mg, ZSM-5 19.2 mg, Hβ 23.6 mg, Amberlyst-15 2 mg), H_2O (10 mL), 150 °C, 4.0 MPa H_2, reaction time 6 h (A) or 4 h (B). Quantified by GC.

Hydration of epoxy alkanes to diols

The hydration of epoxy alkanes is also researched, which is a key reaction route to synthesize various diols that are important intermediates in the fine chemical and pharmaceutical industries [51-54]. To our delight, epoxy styrene is completely transformed with a 99.5% yield of 1,2-dihydroxy styrene after 6 h (Figure 3B, Table 2 entry 1), and diols are the major product of 5 other epoxides (Table 2 entries 2-6). Similarly, the hydrogenated products, i.e., alcohols, following by Markovnikov's rule, were obtained when *n*-hexane was used as a solvent (Table 2 entries 7-12). The reaction was also inactive under a N_2 atmosphere and blank experiment (Figure 3B). Both H_2 and H_2O are necessary for the hydration reaction. This result proves the excellent university of the hydrogen promoting effect on hydration.

Table 2. Hydration of epoxy alkanes to diols.

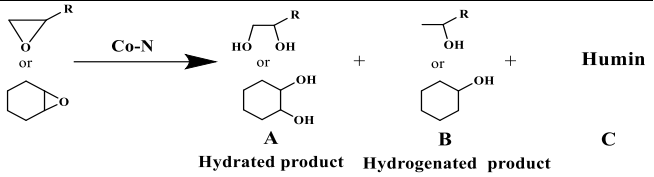

Entry	Alkenes	Conversion (%)	Selectivity (%)		
			A	B	C
1	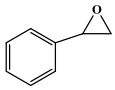	100	99.5		0.5
2	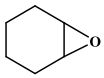	98.5	95.0		5.0
3		86.8	72.9		27.1
4	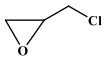	68.7	83.6		16.4
5		58.6	89.3		10.7
6		63.2	68.4		31.6
7	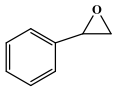	83.5		80.2	19.8
8	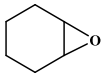	79.6		75.6	24.4
9		50.9		62.5	37.5
10	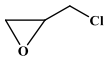	65.6		56.8	43.2
11	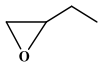	51.4		61.1	38.9
12		52.0		68.3	31.7

Reaction conditions: Epoxides (10 mmol), Co-NC (50 mg), H_2O (10 mL), [7-12]*n*-hexane instead of H_2O, 150 °C, 4.0 MPa H_2, reaction time 4 h. Quantified by GC.

Understanding H_2 promotion

In situ attenuated total reflection infrared (ATR-IR) measurements were performed using D_2 and D_2O as probe molecules to reveal the hydration reaction mechanism. When Co-NC is exposed to D_2 at 150 °C, peaks at 1223 cm^{-1} and 2095 cm^{-1} assigned to the stretching modes of Co-$D^{\delta-}$ and N-$D^{\delta+}$ are observed [55,56], confirming the dissociation of D_2 over the Co-N (Figure 4A). The subsequent introduction of D_2O leads to the generation of the Co-$OD^{\delta-}$ bond (2581 cm^{-1}) and the degradation of Co-$D^{\delta-}$ bond. Meanwhile, the kinetic isotope effect in 3-chlorostyrene hydrogenation was explored with the use of D_2 and *n*-hexane (Figures S7), and the kinetic rate constant using H_2 is 4-5 times higher than that of D_2, indicating

that the H_2 heterolysis activation mechanism is taken place over Co-N [57]. Importantly, the direct interaction of Co-NC with D_2O does not generate such Co-OD$^{\delta-}$ bonds. Meanwhile, the generation of Co-OH$^{\delta-}$ and N-H$^{\delta+}$ can also be indicated by the XPS results of the H_2-H_2O activated sample, which show a shift of Co peak to a lower energy region (779.5, 795.2 eV) and a shift of pyridinic N peak to a higher energy region (398.8 eV) (Figure 1F, G) [58]. The proton hydrogen located on the pyridine N attracts electrons, whereas the hydroxide ion donates electrons, which results in a lower electron density of pyridine N and a higher electron density of Co. The H_2-H_2O-activated Co-NC cannot catalyze hydration under a N_2 atmosphere, and the reused sample shows a similar XPS result to parent Co-NC (Figure 1F, G). These results indicate that the addition of reactant can consume Co-OH$^{\delta-}$ and N-H$^{\delta+}$ bonds, and active sites for hydration reactions must be generated by in situ modification under H_2 and H_2O. To investigate the generality of H_2-promoted hydration for other Co-NCs, $Co_3[Co(CN)_6]_2$-derived Co-NC with a Co content of 1.4 wt% (Table S3) was obtained by a similar method and used in the hydration of 3-chlorostyrene. An increase of the hydration activity in the H_2 atmosphere is also observed (Table S4).

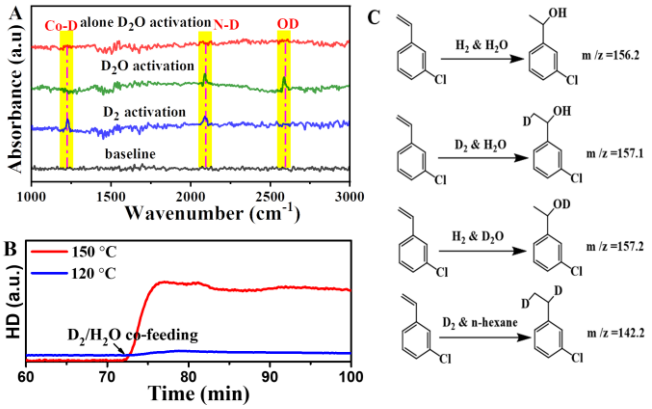

Figure 4. (A) In situ IR spectra for the subsequent D_2 and D_2O activation at 150 °C; (B) MS signals of HD generation during D_2-H_2O treatment; (C) Isotope studies for the hydration and hydrogenation reaction.

Furthermore, significant HD generation is detected by mass spectrometry (MS) when Co-NC is exposed to a mixture of D_2 and H_2O (Figure 4B). A controversy is that the generation of HD is derived from the ion exchange of N-D$^{\delta+}$ with H_2O to N-H$^{\delta+}$ and the subsequent combination of Co-D$^{\delta-}$ and N-H$^{\delta+}$ or the abovementioned conversion of Co-D$^{\delta-}$ and H_2O to Co-OH$^{\delta-}$ [59,60]. The isotopically labeled experimental results analyzed by MS and ^{1}H-NMR show that the hydration of 3-chlorophenylethane generates hydroxyl-deuterated and ethyl-deuterated 1-(3-chlorophenyl)ethanol under D_2-H_2O and H_2-D_2O, respectively (Figure 4C**,** Figures S8, S9). This indicates that H_2O and H_2 contribute OH and H in the hydrated product, and the ion exchange mechanism is weak in the reaction system. Thus, the mechanism of H_2-catalyzed hydration is proposed as follows: (1) H_2 dissociates over Co-N to form Co-H$^{\delta-}$ and N-H$^{\delta+}$ bonds, (2) H_2O is activated over Co-H$^{\delta-}$, in which one of the H$^{\delta+}$ of H_2O couples with H$^{\delta-}$ of the Co-H$^{\delta+}$ to form Co-OH$^{\delta-}$ and a new H_2 molecule, (3) the C=C bond of an alkene is hydrated by Co-OH$^{\delta-}$ and N-H$^{\delta+}$. This means that H_2 plays the role of a catalyst for the acid transformation of the Co-N for the hydration reactions.

Olefin oxidation-reduction for the synthesis of alcohol hydration has been investigated over homogeneous Fe, Co, and Mn-based catalysts under organic solvents, O_2 atmosphere, and reducing agent [61]. The reaction is often consisted of an initial oxidation of olefin to ketone, followed by hydrogenation via a free radical mechanism. Obviously, our catalytic system is significantly different in the aspects of reaction solvent, gas atmosphere, and hydrogen source and reaction mechanism. Despite the milder conditions used over the homogeneous systems, there are envisaged advantages in separation of products from our gas-solid catalyst with higher atom economy and is a greener process: no organic hydrogenation reagent or silane is used, and there is no contamination of soluble metal ions to the products, etc. However, as stated, our system represents a new solid system for hydration in gas phase using the new concept of regenerable FLP sites, which should be evaluated more extensively in future for appropriate comparison to such existing methods. Traditional acid-catalyzed hydration reactions involve protonation of the C=C bond, hydration of the carbenium ion intermediate, and elimination of protons. Usually, the first step is the rate-determining step [62]. In the case of acidic resin and zeolites, H_2O often causes a decrease in acidity and weakens their catalytic ability for alkene protonation [63,64]. In contrast, over Co-NC, H_2O can be activated by a H_2-mediated process and generates N-H bonds with Brønsted acidity, which facilitates the protonation step of the C=C bond. To verify the H_2-catalyzed acid transformation, the acidity and acid type of Co-NC were measured. In NH_3-TPD, Co-NC shows obvious enhancement of the acidity, as indexed by the significant shift of the NH_3 desorption peak from 238 °C to 370 °C after H_2-H_2O activation (Figure S10). Correspondingly, the basicity of the treated catalyst is also found to be altered, according to the results of temperature-programmed desorption of carbon dioxide (CO_2-TPD). In-situ IR spectra of adsorbed pyridine (Py-FTIR) detected at 150 °C show that the parent Co-NC shows pure Lewis acidity with a sole peak at 1450 cm^{-1}, which results from the positive Co$^{\delta+}$ of the Co-NC surface (Figure 5A). The quantified acid concentration ratio was calculated according to the Emeis equation combined with the NH_3-TPD results [65]. After H_2-H_2O activation, a peak at 1540 cm^{-1} attributed to Brønsted acidity appears. The Lewis acid content decreased from 0.159 to 0.085 mmol/g, accompanied by an increase in the Brønsted acid content from 0.002 to 0.075 mmol/g (Table S5). More importantly, the signal detected at 250 °C ascribed to strong acidity indicates an obvious increase in the strong acid amount from 0.043 to 0.063 mmol/g, which is mainly due to the strong acidity of the Brønsted acidity (Figure S11, Table S5). Meanwhile the solid-state ^{31}P MAS NMR measurements of adsorbed trimethylphosphine oxide (TMPO) also show acid transformation, with the parent peak of the Lewis acid site at 54.1 ppm being converted to a Brønsted acid site at 61.0 ppm (Figure 5B) [66]. Previous work shows that the Lewis acidity of MOF can be converted to Brønsted acidity via the coordination of H_2O molecules with metal sites [67]. However, under our reaction conditions, the H_2O pretreatment alone does not causes the H_2O to link to the Lewis Co$^{\delta+}$ sites (Co-O-H$_2$$^{\delta+}$). Meanwhile, the H_2 pretreatment alone did not give any acidity change, which may be attributed to the high reactivity of the in-situ generated H$^{\delta-}$-Co-N-H$^{\delta+}$ [68]. Their instability was further confirmed by XPS, which possesses a similar peaks position of Co and N to parent Co-NC (Figure 1F, G, S12).

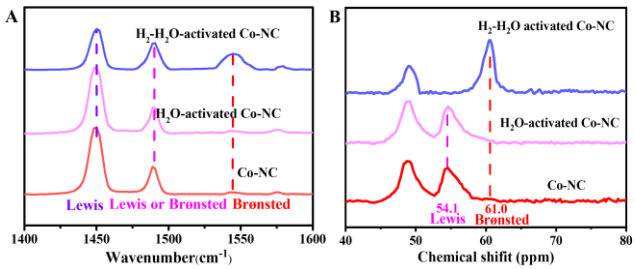

Figure 5. (A) In situ IR spectra of chemisorbed pyridine detected at 150 °C and (B) ^{31}P MAS NMR spectra of chemisorbed adsorbed TMPO for H_2-H_2O-activated Co-NC at 150 °C.

To further understand the unique H_2-catalyzed hydration mechanism, first-principle DFT calculations are performed. A rigid Co-N_4 moiety embedded in the intact graphitic layer is adopted as the model. The DFT calculations show that H_2 is first adsorbed on the Co-N pair, where one H atom is bonded with Co while another is linked to the pyridinic N atom (Figure 6A, B, S13). As a result, H_2 is activated with the H-H bond elongated by 0.188 Å (from the original 0.760 Å to 0.948 Å in TS1). The H_2 dissociation barrier is 0.51 eV, similar to previously reported results [69]. The presence of H_2O does not accelerate H_2 dissociation as the barrier remains nearly the same (0.51 eV *vs*. 0.49 eV). For the dissociation of H_2O, it is adsorbed over N-H to form N-H-O-H_2 with an adsorption energy of -0.28 eV. Subsequently, the electronegative H of Co-$H^{\delta-}$ attacks the electropositive H of adsorbed H_2O, leading to the formation of Co-$OH^{\delta-}$ and a free H_2 molecule. The energy barrier of TS2 is only 0.46 eV, and H_2O dissociation is preferred thermodynamically because the Co-$OH^{\delta-}$ bond is stronger than the Co-$H^{\delta-}$ bond. However, the H_2O dissociative barrier is as high as 1.84 eV without the participation of H_2. The formation of Co-OH and N-H bonds during H_2-catalyzed H_2O dissociation provides a favorable pathway for hydration compared with traditional acid-mediated hydration. As shown in Figure 6B, the hydration of C=C involved two transition states (TS3 by the addition of the first hydrogen atom and TS4 by the addition of H atom or OH group), with barriers of 0.32 eV and 0.28 eV, respectively. In comparison, the direct hydrogenation energy barriers of TS3 and TS4 (TS3 by the addition of the first H atom and TS4 by the addition of the second H atom) are 0.88 eV and 0.81 eV, respectively.

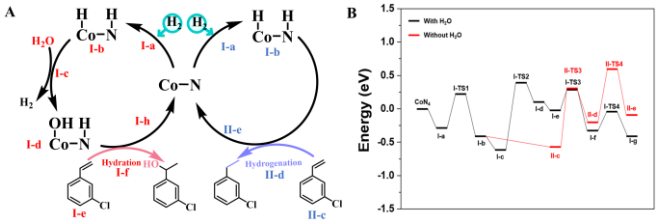

Figure 6. (A) Proposed catalytic reaction mechanism and (B) energy change profile of 3-chlorostyrene hydration and hydrogenation over Co-NC with and without H_2O.

Conclusions

In conclusion, we found an interesting H_2-catalyzed acid-base transformation mechanism from a frustrated Lewis acid-base pair (Co-N) to a Brønsted acid-base pair ($H^{\delta+}$-N-Co-$OH^{\delta-}$) on surface under the mediation of H_2O. The H_2-catalyzed reaction system is superior to traditional catalytic systems over acidic zeolites and resin in the hydration of alkenes and epoxy alkanes. The results identify opportunities for hydrogen-catalyzed acid-base transformation and remove the conceptual barriers between metal hydrogenation and acid catalysis. Although these hydration reactions appear to have suffered from using harsh reaction conditions at this stage, the result clearly implies that the acid catalysis can be conducted without necessarily using conventional acid supports, but, can be triggered by a hydrogenation process. Further follow-up studies are underway. .

Supporting Information

Some catalyst physicochemical properties and catalytic reaction results, Materials, Charecterizations, N_2 adsorption-desorption isotherms, GC-MS patterns, XRD, TEM micrographs, Raman spectra, NH_3-TPD, In situ IR, Configurations of energy change profile, catalytic kinetics, ^{1}H NMR.

Acknowledgments

The authors appreciate the supports from the National Natural Science Foundation of China (22178158, 52162014, 22065024, 21878138), and the Cultivating Project for Academic and Technical Leader of Key Discipline of Jiangxi Province (20212BCJ23038).

References

[1] Zhao, M.; Yuan, K.; Wang, Y.; Li, G.; Guo, J.; Gu, L.; Hu, W.; Zhao, H.; Tang, Z. Metal-organic frameworks as selectivity regulators for hydrogenation reactions. *Nature* **2016**, *539*, 76-80.
[2] Teschner, D.; Borsodi, J.; Wootsch, A.; Révay, Z.; Hävecker, M.; Knop Gericke, A.; Jackson, S. D.; Schlögl, R. The roles of subsurface carbon and hydrogen in palladium-catalyzed alkyne hydrogenation. *Science* **2008**, *320*, 86-89.
[3] Scharnagl, F. K.; Hertrich, M. F.; Ferretti, F.; Kreyenschulte, C.; Lund, H.; Jackstell, R.; Beller, M. Hydrogenation of terminal and internal olefins using a biowaste-derived heterogeneous cobalt catalyst. *Sci. Adv.* **2018**, *4*, 1248.
[4] Welch, G. C.; Juan, R. R. S.; Masuda, J. D.; Stephan, D. W. Reversible, metal-free hydrogen activation. *Science* **2006**, *314*, 1124-1126.
[5] Stephan, D. W. The broadening reach of frustrated Lewis pair chemistry. *Science*, **2016**, *354*, 7229.
[6] Welch, G. C.; Stephan, D.; Facile, W. heterolytic cleavage of dihydrogen by phosphines and boranes. *J. Am. Chem. Soc.* **2007**, *129*, 1880-1881.
[7] Ding, Y.; Huang, X.; Yi, X.; Qiao, Y.; Sun, X.; Zheng, A.; Su, D. S. A heterogeneous metal-free catalyst for hydrogenation: Lewis acid-base pairs integrated into a carbon lattice. *Angew. Chem. Int. Ed.* **2018**, *57*, 13800-13804.
[8] Bauer, H.; Alonso, M.; Fischer, C.; Rçsch, B.; Elsen, H.; Harder, S. Simple alkaline-earth metal catalysts for effective alkene hydrogenation. *Angew. Chem. Int. Ed.* **2018**, *57*, 15177-15182.
[9] Zhang, S.; Huang, Z. Q.; Ma, Y.; Gao, W; Li, J; Cao, F.; Li, L.; Chang, C. R.; Qu, Y. Solid frustrated-Lewis-pair catalysts constructed by regulations on surface defects of porous nanorods of CeO_2. *Nat. Commun.* **2017**, *8*, 15266.
[10] Liu, D.; Yang, P.; Zhang, H.; Liu, M.; Zhang, W.; Xu, D.; Gao, J. Direct reductive coupling of nitroarenes and alcohols catalysed by Co-N-C/CNT@AC. *Green Chem.* **2019**, *21*, 2129-2137.
[11] Zhou, P.; Jiang, L.; Wang, F.; Deng, K.; Lv, K.; Z. Zhang, High performance of a cobalt-nitrogen complex for the reduction and reductive coupling of nitro compounds into amines and their derivatives. *Sci. Adv.* **2017**, *3*, 1601945.
[12] Zhang, F.; Zhao, C.; Chen, S.; Li, H.; Yang, H.; Zhang, X. M. In situ mosaic strategy generated Co-based N-doped mesoporous carbon for highly selective hydrogenation of nitroaromatics. *J. Catal.* **2017**, *348*, 212-222.
[13] Korstanje, T. J.; van der Vlugt, J. I.; Elsevier, C. J.; de Bruin, B. Hydrogenation of carboxylic acids with a homogeneous cobalt catalyst. *Science* **2015**, *350*, 298-302.
[14] Corma, A. From microporous to mesoporous molecular sieve materials and their use in catalysis. *Chem. Rev.* **1997**, *97*, 2373-2420.
[15] Konwar, L. J.; Mäki-Arvela P., Mikkola J. P.; SO_3H-containing functional carbon materials: synthesis, structure, and scid catalysis. *Chem. Rev.* **2019**, *119*, 11576-11630.
[16] Zhong, Y.; Deng, Q.; Yao, Q.; Lu, C.; Zhang, P.; Li, H.; Wang, J.; Zeng, Z.; Zou, J. J.; Deng, S. Functionalized biochar with superacidity

and hydrophobicity as a highly efficient catalyst in the synthesis of renewable high-density fuels. *ACS Sustainable Chem. Eng.* **2020**, *8*, 7785−7794.
[17] Du Z.; Shao, Z. Combining transition metal catalysis and organocatalysis-an update. *Chem. Soc. Rev.* **2013**, *42*, 1337-1378.
[18] Zhang, J.; Ellis, L. D.; Wang, B; Dzara, Michael J.; Sievers, C.; Pylypenko, S.; Nikolla E.; Will Medlin, J. Control of interfacial acid-metal catalysis with organic monolayers. *Nature Catal.* **2018**, *1*, 148–155.
[19] Jin, X.; Tsukimura, R.; Aihara, T.; Miura, H.; Shishido, T.; Nozaki, K. Metal-support cooperation in $Al(PO_3)_3$-supported platinum nanoparticles for the selective hydrogenolysis of phenols to arenes. *Nature Catal.* **2021**, *4*, 312-321.
[20] Triwahyono, S.; Jalil, A.; Ruslan, N. N.; Setiabudi, H.; Kamarudin, N. C_5-C_7 linear alkane hydroisomerization over MoO_3-ZrO_2 and Pt/MoO_3-ZrO_2 catalysts. *J. Catal.* **2013**, *303*, 50-59.
[21] Ebitani, K.; Tsuji, J.; Hattori, H.; Kita, H. Dynamic modification of surface acid properties with hydrogen molecule for zirconium oxide promoted by platinum and sulfate ions. *J. Catal.* **1992**, *135*, 609-617.
[22] Triwahyono, S.; Yamada, T.; Hattori, H. IR study of acid sites on WO_3-ZrO_2 and Pt/WO_3-ZrO_2. *Appl. Catal. A: Gen.* **2003**, *242*, 101-109.
[23] Ebitani, K.; Konishi, J.; Hattori, H. Skeletal isomerization of hydrocarbons over zirconium oxide promoted by platinum and sulfate ion. *J. Catal.* **1991**, *130*, 257-267
[24] Watanabe, K.; Oshio, N.; Kawakami, T.; Kimura, T. Isomerization reactions with sulfur-containing pentane over Metal/SO_4^{2-}/ZrO_2 catalysts. *Appl. Catal. A: Gen.* **2004**, *272*, 281–287.
[25] Toshihide, B.;Yoshio, O. Hydrogen induced catalysis by silver-exchanged zeolites: transformation of ethylbenzene over AgY zeolite, *Zeolites*, **1987**, *7*, 292-294.
[26] Wang, A.; Li, J.; Zhang, T. Heterogeneous single-atom catalysis. *Nat. Rev. Chem.* **2018**, *2*, 65-81.
[27] Ji, S.; Chen, Y.; Wang, X.; Zhang, Z.; Wang D.; Li Y. Chemical synthesis of single atomic site catalysts. *Chem. Rev.* **2020**, *120*, 11900-11955
[28] Wang, Y; Su, H; He, Y.; Li, L.; Zhu, S.; Shen, H; Xie, P; Fu, X.; Zhou, G.; Feng, C.; Zhao, D.; Xiao, F.; Zhu, X.; Zeng, Y.; Shao, M.; Chen, S.; Wu, G.; Zeng, J.; Wang C.; Advanced electrocatalysts with single-metal-atom active sites. *Chem. Rev.* **2020**, *120*, 12217-12314
[29] Peeters, A.; Valvekens, P.; Ameloot, R.; Sankar, G.; Kirschhock, C. E. A.; Vos, D. E. D. Zn-Co double metal cyanides as heterogeneous catalysts for hydroamination: a structure-activity relationship. *ACS Catal*. **2013**, *3*, 597-607.
[30] Feng, Y.; Yu, X. Y.; Paik, U. Formation of Co_3O_4 microframes from MOFs with enhanced electrochemical performance for lithium storage and water oxidation. *Chem. Commun.* **2016**, *52*, 6269-6272.
[31] Kresse, G.; Hafner, J. Ab initio molecular dynamics for liquid metals. *Phys. Rev. B* **1993**, *47*, 558-561.
[32] Perdew, J. P.; Burke, K.; Ernzerhof, M. Generalized gradient approximation made simple. P*hys. Rev. Lett.* **1996**, *77*, 3865-3868.
[33] Mathew, K.; Sundararaman, R.; Letchworth-Weaver, K.; Arias, A. A.; Hennig, R. G. Implicit solvation model for density-functional study of nanocrystal surfaces and reaction pathways. *J. Chem. Phys.* **2014**, *140*, 084106.
[34] Gauthier, J. A.; Dickens, C. F.; Heenen, H. H.; Vijay, S.; Ringe, S.; Chan, K. Unified approach to implicit and explicit solvent simulations of electrochemical reaction energetic. *J. Chem. Theory Comput.* **2019**, *15*, 6895-6906.
[35] Zhong, W.; Liu, H.; Bai, C.; Liao, S.; Li, Y. Base-free oxidation of alcohols to esters at room temperature and atmospheric conditions using nanoscale Co-based catalysts. *ACS Catal.* **2015**, *5*, 1850-1856.
[36] He, Y.; Hwang, S.; Cullen, D. A.; Uddin, M. A.; Langhorst, L.; Li, B.; Karakalos, S.; Kropf, A. J.; Wegener, E. C.; Sokolowski, J.; Chen, M.; Myers, D.; Su, D.; More, K. L.; Wang, G.; Litster, S.; Wu, G. Highly active atomically dispersed CoN_4 fuel cell cathode catalysts derived from surfactant-assisted MOFs: carbon-shell confinement strategy. *Energy Environ. Sci.* **2019**, *12*, 250-260.
[37] Sabhapathy, P.; Liao, C. C.; Chen, W. F.; Chou, T. C.; Shown, I.; Sabbah, A.; Lin, Y. G.; Lee, J. F.; Tsai, M. K.; Chen, K. H.; Chen, L. C. Highly efficient nitrogen and carbon coordinated N-Co-C electrocatalysts on reduced graphene oxide derived from vitamin-B_{12} for the hydrogen evolution reaction. *J. Mater. Chem. A* **2019**, *7*, 7179-7185.
[38] Zhang, H.; Zhou, W.; Chen, T.; Guan, B.; Li, Z.; Lou, X. W. A modular strategy for decorating isolated cobalt atoms into multichannel carbon matrix for electrocatalytic oxygen reduction. *Energy Environ. Sci.* **2018**, *11*, 1980.
[39] Jensen, C. M.; Trogler, W. C. Catalytic hydration of terminal alkenes to primary alcohols,. *Science* **1986**, *233*, 1069-1071.
[40] Dong, G.; Teo, P.; Wickens, Z. K.; Grubbs, R. H. Primary alcohols from terminal olefins: formal anti-Markovnikov hydration via triple relay catalysis. *Science* **2011**, *333*, 1609-1612.
[41] Zhang, X.; Deng, Q.; Han, P.; Xu, J.; Pan, L.; Wang, L.; Zou, J. J. Hydrophobic mesoporous acidic resin for hydroxyalkylation/alkylation of 2-methylfuran and ketone to high-density biofuel. *AIChE J.* **2017**, *63*, 680-688.
[42] Bianchini, E.; Pietrobon, L.; Ronchin, L.; Tortato, C.; Vavasori, A. Trifluoroacetic acid promoted hydration of styrene catalyzed by sulfonic resins: comparison of the reactivity of styrene, n-hexene and cyclohexene. *Appl. Catal. A: Gen.* **2019**, *570*, 130-138.
[43] Zhang, H.; Mahajani, S. M.; Sharma, M. M.; Sridhar, T. Hydration of cyclohexene with solid acid catalysts. *Chem. Eng. Sci.* **2002**, *57*, 315-322.
[44] Nuntasri, D.; Wu, Peng; Tatsumi, T. Highly selective formation of cyclopentanol through liquid-phase cyclopentene hydration over MCM-22 catalysts. *Chem. Lett.* **2002**, *31*, 224-225.
[45] Yuan, P. Q.; Liu, Y.; Bai, F.; Xu, L.; Cheng, Z. M.; Yuan, W. K. Hydration of cyclohexene in sub-critical water over WO_x-ZrO_2 catalysts. *Catal. Commun.* **2011**, *12*, 753-756.
[46] Nuntasri, D.; Wu, P.; Tatsumi, T High selectivity of MCM-22 for cyclopentanol formation in liquid-phase cyclopentene hydration. *J. Catal.* **2003**, *213*, 272-280.
[47] Chwang, W. K.; Nowlan, V. J.; Tidwell, T. T. Reactivity of cyclic and acyclic olefinic hydrocarbons in acid-catalyzed hydration. *J. Am. Chem. Soc.* **1977**, *99*, 7233-7238.
[48] Panneman, H. J.; Beenackers, A. A. C. M. Effect on the hydration of cyclohexene catalyzed by strong ion-exchange resins. 2. Effect of sulfolane on the reaction kinetics, *Ind. Eng. Chem. Res.* **1992**, *31*, 1425-1433.
[49] Sun, W.; Zhang, Xu; Hou, Y.; Wang, Y.; Wang, X.; Xue, W. Polystyrene-based hierarchically macro-mesoporous solid acid: a robust and highly efficient catalyst for indirect hydration of cyclohexene to cyclohexanol by a one-pot method under mild conditions. *Ind. Eng. Chem. Res.* **2020**, *59*, 6435-6444.
[50] Cao, Z. J.; Zhao, X.; He, F. Q.; Zhou, Y.; Huang, K.; Zheng, A. M.; Tao, D. J. Highly efficient indirect hydration of olefins to alcohols using superacidic polyoxometalate-based ionic hybrids catalysts. *Ind. Eng. Chem. Res.* **2018**, *57*, 6654-6663.
[51] Tokunaga, M.; Larrow, J. F.; Kakiuchi, F.; Jacobsen, E. N. Asymmetric catalysis with water: efficient kinetic resolution of terminal epoxides by means of catalytic hydrolysis. *Science* **1997**, *277*, 936-938.
[52] Tang, B.; Dai, W.; Wu, G.; Guan, N.; Li, L.; Hunger, M. Improved postsynthesis strategy to Sn-beta zeolites as Lewis acid catalysts for the ring-opening hydration of epoxides. *ACS Catal.* **2014**, *4*, 2801-2810.
[53] Dai, W. Wang, C.; Tang, B. Wu, G.; Guan, N.; Xie, Z.; Hunger, M.; Li, L. Lewis acid catalysis confined in zeolite cages as a strategy for sustainable heterogeneous hydration of epoxides. *ACS Catal.* **2016**, *6*, 2955-2964.
[54] Li, Bo; Bai, S.; Wang, X.; Zhong, M.; Yang, Q.; Li C. Hydration of Epoxides on [Co^{III}(salen)] Encapsulated in Silica-Based Nanoreactors. *Angew. Chem. Int. Ed.* **2012**, *51*, 11517-11521.
[55] Billups, W. E.; Chang, S. C.; Hauge, R. H.; Margrave, J. L. Low-temperature reactions of atomic cobalt with CH_2N_2, CH_4, CH_3D, CH_2D_2, CHD_3, CD_4, H_2, D_2, and HD. *J. Am. Chem. Soc.* **1995**, *117*, 1387-1392.
[56] Wallin, M.; Gro1nbeck, H.; Spetz, A. L.; Eriksson, M.; Skoglundh, M. Vibrational analysis of H_2 and D_2 adsorption on Pt/SiO_2. *J. Phys. Chem. B* **2005**, *109*, 9581-9588.
[57] Liu, P.; Zhao, Y.; Qin, R.; Mo, S.; Chen, G.; Gu, L.; Chevrier, D. M.; Zhang, P.; Guo, Q.; Zang, D.; Wu, B.; Fu, G.; Zheng, N. Photochemical route for synthesizing atomically dispersed palladium catalysts. *Science* **2016**, *352*, 797-800.
[58] Huang, K.; Fu, H.; Shi, W.; Wang, H.; Cao, Y.; Yang, G.; Peng, F.; Wang, Q.; Liu, Z.; Zhang, B.; Yu, H. Competitive adsorption on single-atom catalysts: mechanistic insights into the aerobic oxidation of alcohols over Co-N-C. *J. Catal.* **2019**, *377*, 283-292.

[59] Zhao, Z.; Bababrik, R.; Xue, W.; Li, Y.; Briggs, N. M.; Nguyen, D. T.; Nguyen, U.; Crossley, S. P.; Wang, S.; Wang, B.; Resasco, D. E. Solvent-mediated charge separation drives alternative hydrogenation path of furanics in liquid water. *Nature Catal.* **2019**, *2*, 431-436.
[60] Dai, Y.; Gao, X.; Chu, X.; Jiang, C.; Yao, Y.; Guo, Z.; Zhou, C.; Wang, C.; Wang, H.; Yang, Y.; On the role of water in selective hydrogenation of cinnamaldehyde to cinnamyl alcohol on PtFe catalysts. *J. Catal.* **2018**, *364*, 192-203.
[61] Crossley, S. W. M.; Obradors, C.; Martinez, R. M.; Shenvi, R. A. Mn-, Fe-, and Co-catalyzed radical hydrofunctionalizations of olefins, *Chem. Rev*. **2016**, *116*, 8912-9000.
[62] Izumi, Y. Hydration/hydrolysis by solid acids. *Catal. Today* **1997**, *33*, 371-409.
[63] Da Silva Rocha, K. A.; Hoehne, J. L.; Gusevskaya, E. V. Phosphotungstic acid as a versatile catalyst for the synthesis of fragrance compounds by a-pinene oxide isomerization: solvent-induced chemoselectivity. *Chem. Eur. J*. **2008**, *14*, 6166-6172.
[64] Morales, G.; Athens, G.; Chmelka, B. F.; Grieken, R. V.; Melero, J. A. Aqueous-sensitive reaction sites in sulfonic acid-functionalized mesoporous silicas, *J. Catal*. **2008**, *254*, 205-217.
[65] Emeis, C. A. Determination of integrated molar extinction coefficients for infrared absorption bands of pyridine adsorbed on solid acid catalysts, *J. Catal*. **1993**, *141*, 347-354.
[66] Zheng, A.; Liu, S. B.; Deng, F. ^{31}P NMR chemical shifts of phosphorus probes as reliable and practical acidity scales for solid and liquid catalysts. *Chem. Rev*. **2017**, *117*, 12475.
[67] Hall, J. N.; Bollini, P. Metal-organic framework MIL-100 catalyzed acetalization of benzaldehyde with methanol: Lewis or Brønsted acid catalysis, *ACS Catal*. **2020**, *10*, 3750-3763.
[68] Liu, W.; Zhang, L.; Yan, W.; Liu, X.; Yang, X.; Miao, S.; Wang, W.; Wang, A.; Zhang, T. Single-atom dispersed Co-N-C catalyst: structure identification and performance for hydrogenative coupling of nitroarenes. *Chem. Sci.* **2016**, *7*, 5758-5764.
[69] Liu, W.; Chen, Y.; Qi, H.; Zhang, L.; Yan, W.; Liu, X.; Yang, X.; Miao, S.; Wang, W.; Liu, C.; Wang, A. A durable nickel single-atom catalyst for hydrogenation reactions and cellulose valorization under harsh conditions. *Angew. Chem. Int. Ed.* **2018**, *57*, 7071-7075.

Graphic for manuscript